



Depositional Record and Geochemistry Constraints on the Late Miocene–Quaternary Evolution of the Taiyuan Basin in Shanxi Rift System, China

Qitian Zhuang^{1,2}, Rongzhu Wei³ and Honglin He^{1,2*}

¹State Key Laboratory of Earthquake Dynamics, Institute of Geology, China Earthquake Administration, Beijing, China, ²Shanxi Taiyuan Continental Rift Dynamics National Observation and Research Station, Taiyuan, China, ³Shanxi Institute of Geological Survey, Taiyuan, China

OPEN ACCESS

Edited and reviewed by:

Xuhua Shi,
Zhejiang University, China

*Correspondence:

Honglin He
honglinhe123@vip.sina.com

Specialty section:

This article was submitted to
Quaternary Science, Geomorphology
and Paleoenvironment,
a section of the journal
Frontiers in Earth Science

Received: 11 December 2021

Accepted: 24 January 2022

Published: 09 March 2022

Citation:

Zhuang Q, Wei R and He H (2022)
Depositional Record and
Geochemistry Constraints on the Late
Miocene–Quaternary Evolution of the
Taiyuan Basin in Shanxi Rift
System, China.
Front. Earth Sci. 10:833585.
doi: 10.3389/feart.2022.833585

The formation and evolution of the Shanxi Rift System are topics of interest because of its unique geometry and critical position in the North China Plate. However, it is not easy to delineate the late Cenozoic tectonic processes. This is partly because it is difficult to preserve the normal faults' movement evidence and related deposits for dating in the outcrop. Besides, the current studies are heavily weighted in the low-temperature thermochronology, whereas it is insensitive to the exhumation after the late Miocene. To decipher the late Cenozoic evolution, we offer a case of detailed depositional recording from the boreholes of the Taiyuan Basin in the Shanxi Rift System. Fluvial, deltaic, and lacustrine environments were identified by the systematic stratigraphic analysis of boreholes. Two mega transgressions generated basin-wide lakes at ca. 5.8–4.4 and ca. 2.2–1.6 Ma. We attribute the lake expansion events to tectonism because climatic variations from reconstruction of the paleoclimate with geochemistry index and previous work exhibited asynchronous processes with the transgression. Thus, the basin experienced two stages of extensive subsidence after the rift occurred. This result is conducive to obtaining a more complete late Cenozoic tectonic evolution of the Shanxi Rift System.

Keywords: shanxi rift system, cenozoic, geochemistry, sedimentary environment, palaeoclimate

1 INTRODUCTION

The Cenozoic intracontinental extension around the Ordos Block of the western North China Plate is a significant component of the Eurasian continent deformation (Tapponnier and Molnar, 1977; Tapponnier et al., 1982; Peltzer et al., 1985; Yin, 2010). A range of basins have been generated since the early Eocene in the periphery of the Ordos Block, and they are commonly related to the evolution of the Tibet Plateau (Deng et al., 1973; Tapponnier and Molnar, 1977; Ma et al., 1982; Tapponnier et al., 1986; Zhang et al., 2003; Kusky et al., 2007). The Shanxi Rift System, which situates in the east margin of the Ordos Block, is usually believed as the latest formed basin system (Zhang et al., 1998; Deng et al., 1999; Wei et al., 2020). Therefore, discrepancies of development time and evolution processes between the Shanxi Rift System and other basins around the Ordos Block have drawn researchers' attentions (The Research Group on Active Fault System around Ordos Massif State

Seismological Bureau, 1988; Xu and Ma, 1992; Zhang et al., 1998; Zhang et al., 2003; Zhang et al., 2006; Shi et al., 2020), and this raises the need for an integrated knowledge of the rift evolution.

Works of predecessors, such as the low-temperature thermochronology (Li Bin et al., 2015; Zhao et al., 2016; Chang et al., 2018; Clinkscales et al., 2020; Clinkscales et al., 2021; Su et al., 2021), revealed that the rift could have experienced multiple uplift events from the Late Cretaceous to Miocene. However, it is challenging to constrain the cooling history after Miocene due to the annealing temperature limitation. In addition, analysis of fault kinematics (Zhang et al., 1998; Zhang and Liao, 2006; Shi et al., 2015; Shi et al., 2020) presented the regional stress transition of multiple phases, illustrating the Pacific Plate and/or Indian Plate dynamic source. Nevertheless, most of the results above were more likely to delineate the pre-rift episodes than the syn-rift processes since no corresponding deposits prior to the mid-Miocene were found in the Shanxi Rift System (Wei et al., 2020). On the other hand, detailed sedimentology researches are mainly from limited and incomplete outcrops (Sun, 2005; Deng et al., 2007; Liu et al., 2012; Chen et al., 2016; Chen et al., 2021), which is insufficient for a comprehensive understanding of the evolution. Hence, analysis based on a complete depositional succession in the basin is vital in basin evolution research (Liu and Zhang, 2005). Furthermore, it requires the establishment of the basin filling succession and the sedimentary environment evolution.

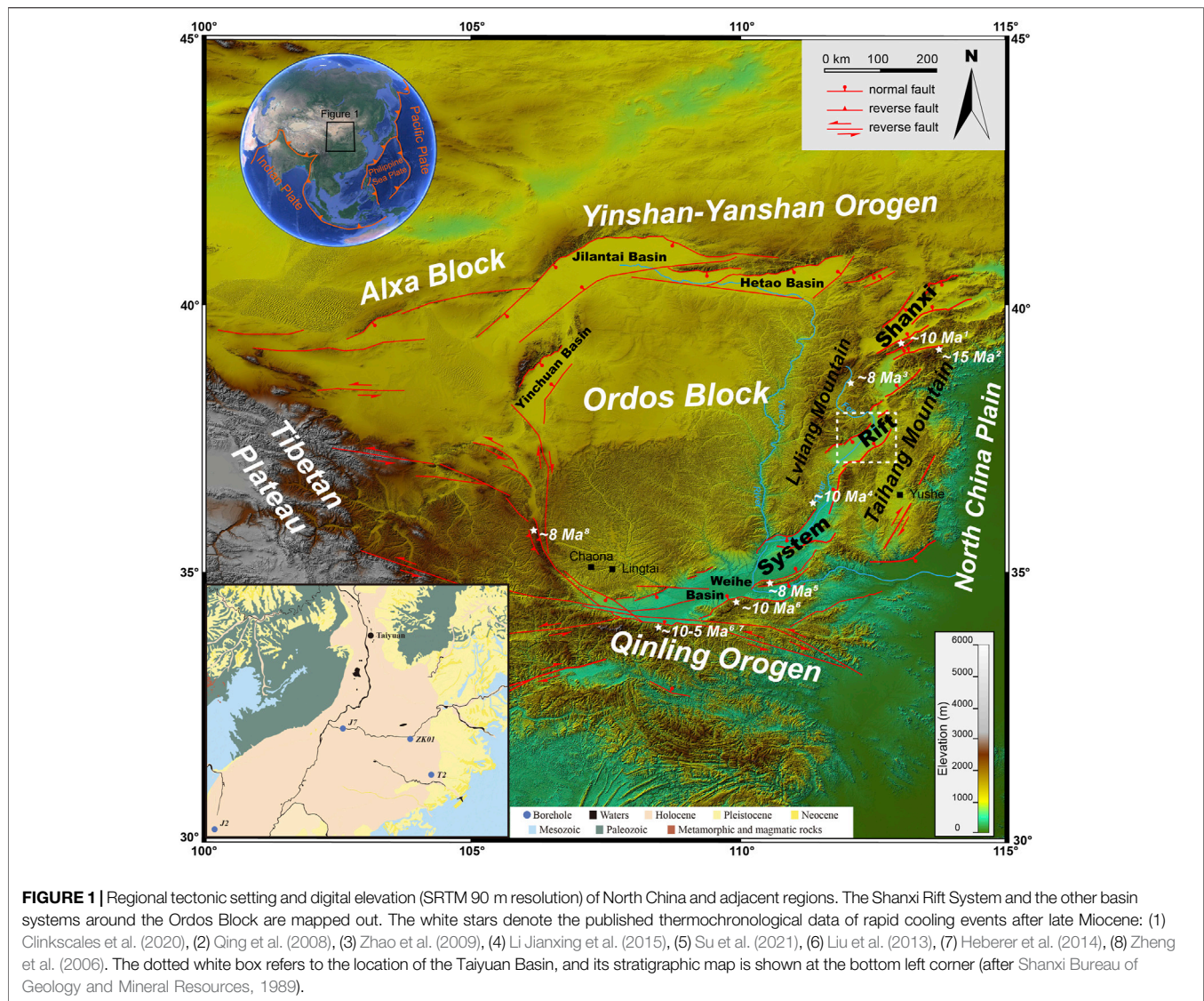
Sedimentary basins are regions of prolonged subsidence on Earth's surface (Allen and Allen, 2013). Subsidence provides accommodation for the storage of detritus from adjacent ranges suffering weathering and erosion (Allen and Allen, 2013). While the sediments, in turn, record the history of mountain uplift and the degree of weathering in the source area. Therefore, there is an inextricably linked liaison between climate, process of denudation–transportation–deposition, and tectonic settings in the basin-range research field (Zhang et al., 2001; Pan et al., 2003; Weltje and Von Eynatten, 2004; Clift and Jonell, 2021).

In order to obtain a complete sedimentary sequence, we conducted borehole ZK01 in the east part of Taiyuan Basin, which lies in the middle of the Shanxi Rift System. The geochemistry of sediments from the drill was analyzed to reveal the palaeoenvironment (Singer, 1980; Armstrong-Altrin, 2009; Wang et al., 2021) of the Taiyuan Basin. In addition, many boreholes have been carried out by the Shanxi Oil Team before ZK01. Thereinto, borehole J2, J7, and T2 perforate the Cenozoic and are distributed in different basin parts. Although their age data are absent, a relatively detailed record compiling can be used to stratigraphic division and correlation, which is helpful for a more integrated study of the evolution of Taiyuan Basin. We aim to fetch the palaeoenvironment information *via* elements analysis, and then recognize the sedimentary environments and establish the sedimentary sequence in Taiyuan Basin. Furthermore, we attempt to discuss whether the shifts of the environments result from climate-driven or tectonic-driven processes.

2 GEOLOGICAL SETTING

The Shanxi Rift System is located on the eastern margin of the Ordos basin and the west side of the North China Plain (Figure 1). The rift system terminates at the Yinshan–Yanshan (“shan” = mountain) orogenic belt on the north and is connected with Weihe Basin and Qinling Mountain on the south. The western Lvliang Mountain and eastern Taihang Mountain separate the Ordos basin and the North China Plain from the Rift System, respectively. According to the drill data (Xu et al., 1993; Wei et al., 2020; Yan et al., 2020), aeolian red clay and gravels (Xu et al., 2009; Yue et al., 2004), and the Cenozoic basalt (Chen, 1987; Wang et al., 1996), the Shanxi Rift System were developed from late Miocene. The thermochronologic data also denoted the time of the most recent rapid cooling event around the Shanxi Rift System at about 10 Ma (white stars and time labels in Figure 1). A total of five en echelon basins (from north to south, Datong Basin, Xin-Ding Basin, Taiyuan Basin, Linfen Basin, and Yuncheng Basin) in left stepped form extend for >700 km. Basins are separated by mountain or push-up swells (Xu and Ma, 1992; Xu et al., 1993). The range-front steep faults, as the boundaries between ranges and basins, are characterized by dip-slip and perhaps accompanied by a small amount of dextral strike-slip component (Hu et al., 2012; Jiang et al., 2012; Xu, 2012; Zhang and Liu, 2012; Huang et al., 2018). The active normal faults control the subsidence of basins, and the maximal thickness of Cenozoic sediments is more than 4 km (Xu and Ma, 1992). Although the active faults are believed only started in late Neogene (Wang et al., 1996; Zhang et al., 1998; Zhang et al., 2003), the location and geometry of the basins are likely to be dependent in part on the pre-existing fold-thrust belt structures (Clinkscales and Kapp, 2019) of the Indosinian (235–200 Ma old) orogeny and the Yanshanian (150–60 Ma old) orogeny (Xu and Ma, 1992; Xu et al., 1993; Zhang et al., 1998).

The Taiyuan Basin lies in the central part of the Shanxi Rift System. Two high-angle normal faults on the NW (i.e., the Jiaocheng Fault) and SE sides (i.e., the Taigu Fault) restrict the basin in a typical rhombic shape (Xu et al., 1993). The striking difference between the sedimentary thickness of the western and eastern part of the basin indicates asymmetrical subsidence (Zhang et al., 1998; Shi et al., 2015; Wei et al., 2020), revealing that the Jiaocheng Fault is more active than the Taigu Fault. The Fen River originates from the northern Lvliang Mountain, passing through the Jiaocheng Fault into Taiyuan Basin, then joining the Yellow River further downstream. Deep incised meander is created in Lvliang Mountain before where the Fen River drains into the basin. In the north, the Shilingguan Uplift occurs in the joint of the Taiyuan Basin and the Xin-Ding Basin, consisting mainly of Paleozoic limestone and overlying Quaternary unconsolidated deposits (Shanxi Bureau of Geology and Mineral Resources, 1989; Wang et al., 1996). It is disputed that whether the Shilingguan Uplift was a paleocourse of Hutuo River into Taiyuan Basin from Xin-Ding Basin or not (Willis, 1907; Li and Liang, 1965; Cheng, 1983; Wu, 1996). In the south, the Fen River flows into the Linfen Basin through the narrow Lingshi Uplift, cutting a canyon with hundreds of meters



in height in the Paleozoic strata. Pre-Cenozoic strata form the main body of surrounding ranges. Nevertheless, the Archean–Paleoproterozoic igneous and metamorphic basement rocks are exposed mainly to the north of the Taiyuan Basin and in the southernmost of the Shanxi Rift System, as well as the low-grade metamorphic Proterozoic rocks (Shanxi Bureau of Geology and Mineral Resources, 1989). Unlike the Precambrian rocks, Paleozoic marine–continental strata and Mesozoic fluvial-lacustrine strata are widely distributed with a dominant position. The pre-Cenozoic strata were folded to form the northeast-southwest trending Taihang-Lvliang fold belt in Yanshanian (Clinkscales and Kapp, 2019). Afterward, the fold belt was unconformably covered by late Cenozoic deposits. Around the Taiyuan Basin, most of the Cenozoic sediments are buried in the basin with a depth up to 4,000 m (Xu et al., 1993; Wang et al., 1996). The residual outcrop of Cenozoic sediments is primarily in the eastern piedmont platform.

However, rare outcrop can be seen around the west rim of Taiyuan Basin (Wang et al., 1996), which may have a causal link with the intense activity of the Jiaocheng Fault. The paleomagnetic chronology of the bottom sediments in Taiyuan Basin presents ca. 8.1 Ma (Wei et al., 2020), manifesting a late Miocene sedimentary formation.

3 STRATIGRAPHY AND SEDIMENTARY ENVIRONMENTS

3.1 Stratigraphy

The ZK01 drill hole locates in the northeastern part of the Taiyuan Basin (Figure 1). A total length of 850 m of borehole core reveals a complete Cenozoic stratigraphic succession of Taiyuan Basin. From bottom to top, the section is divided into six formations [i.e., Xiatuhe Formation (Xt Fm.), Xiaobai

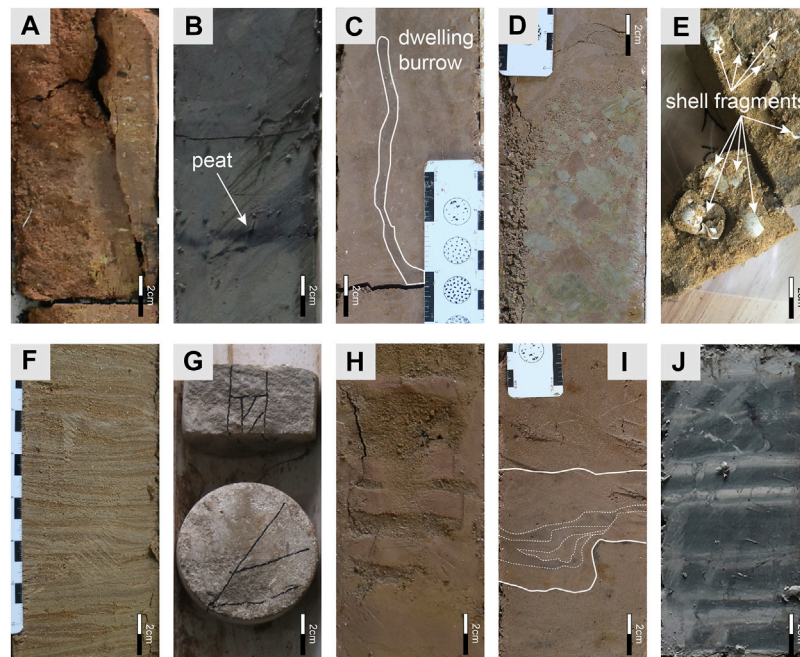


FIGURE 2 | Photographs of typical sedimentary features in ZK01 core. **(A)** Paleosol in Xiatuhe Formation (Xt Fm.). **(B)** Black organic-rich clay in Xiaobai Formation (Xb Fm.). Note the peat layer to which the arrow points. **(C)** Mud-filled dwelling burrow in Hongya Formation (Hy Fm.). **(D)** Mud clasts in Hy Fm., with rough normal-grading. **(E)** Shell fragments in Dagou Formation (Dg Fm.). **(F)** Wavy beddings of sand and clayey silt in Mugua Formation (Mg Fm.). **(G)** Rigid and compact calcareous cement in Fenhe Formation (Fh Fm.). **(H)** Contorted beds commonly seen on delta front. **(I)** Tidal rhythmite consisting of silts and muds. **(J)** Lacustrine rhythmite of pale carbonate-rich and dark organic-rich stratifications.

Formation (Xb Fm.), Hongya Formation (Hy Fm.), Dagou Formation (Dg Fm.), Mugua Formation (Mg Fm.), and Fenhe Formation (Fh Fm.) (Wei et al., 2020).

3.1.1 Xiatuhe formation (853–584 m)

The Xt Fm. is unconformably overlaid on the Yanchang Formation of the Upper Triassic, with a thickness of 270 m. The lower part (853–788 m) is characterized by brown pebbles and sands that alternate stratigraphically. Erosional surfaces are common at the base of the coarse fraction. The pebbles are moderately to well rounded and mainly composed of sandstone. The sands range from silts to coarse sands with poor sorting. It is worth noting that an interval of paleosol is recorded between the pebble layers (Figure 2A). A decrease of particle size occurs upward to form a granule–silt succession. The upper part (788–584 m) consists of massive light brick-red silts and clayey silts, with a few thin clay interlayers. The silts are granularity uniform and enriched with calcium masses. The deposits are colored light red by iron oxides. Besides, mud-clasts are common, implying the presence of high-energy flows. Fossils are rarely found.

3.1.2 Xiaobai formation (584–399 m)

As the finest section on granularity in the whole drill core, the lower part (584–508 m) of Xb Fm. is whitish-gray to gray-olive-green clay in the majority, while the upper part (508–399 m) includes dark gray-green clay and pale brown silts–silty clay. Rhythmites are common in the lower part. On the whole, this

section presents a coarsening-upward tendency. The pale gray color of the sediment may be attributed to the large amount of calcium it contains, which has a remarkable distinction with the underlying light brick-red Xt Fm. Most of the Xb Fm. sections are massive thick layers, with a handful of finely laminated rhythmites. The fragments of *Corbicula*, which live in freshwater are common. Black organic-rich clay layers appear on the upper part of the section (Figure 2B).

3.1.3 Hongya Formation (399–264 m)

The Hy Fm. has a large particle size variation. It starts with pebbly medium sand of normal grading and is overlaid by brown massive clay–silty clay (399–338 m). The middle part (338–320 m) is featured by dark brown silts–medium sands interbedded with silty clay. Many rust-colored spots appear in the silty clay. There are mud-filled dwelling burrows perpendicular to the bedding in the silts at the top of this part (Figure 2C). This part constitutes the coarsest-grained fraction in the Hy Fm. The upper part (320–264 m) comprises gray-brown silts and clay. Yellowish green spots are observed in clay layers. A 10-cm-thick layer of pebble-shaped mud clasts is sandwiched between silt layers. The mud clasts are poorly sorted and subangular, with irregular bedding planes (Figure 2D). The Hy Fm. contains a small amount of *Viviparus*.

3.1.4 Dagou formation (264–182)

The Dg Fm. is also characterized by a fusiform granularity distribution pattern. At the bottom (264–246 m), gray and

dark brown silty clay is the majority, with a thin bed of weakly developed cross-lamination. A large number of shell fragments are visible. The coarse part (246–215 m) consists mainly of brown fine sands and silts. Rounded granules are sporadic in pure and closely graded sands, usually with distinct normal grading. Erosion surfaces are common on the bottom of the normal grading sequences. The upper part (215–182) consists of light brown silts and silty clay, with few thin layers of fine sands. This part is marked by plentiful yellowish-green mottles, bands, and masses. Laminated structures can be seen in intercalated thin silts and clay, which may be attributed to climatic variations. The silts usually have a sharp base and lenticular form, presenting ripples on their upper surface. Abundant shell fragments (**Figure 2E**) are visible in silts.

3.1.5 Mugua formation (182–127 m)

The Mg Fm. is composed mainly of brown to grayish-black clay and silty clay. Plentiful broken shells spread among very thin fine sand layers. In the lower part (172–173), massive rust stains are very extensive. Parallel beddings are well developed, especially in the finest portion. In the upper part of the formation, black organic-rich bands are common in the gray clay unit. The well-developed wavy beddings of sand and clayey silt occur at the top (**Figure 2F**).

3.1.6 Fenhe formation (127–0 m)

Brown and beige silty clay–silts and fine sands are the central features of the Fh Fm. Noteworthy increase of sand content differs significantly from the underlying Mg Fm., which is mainly clay and silty clay. It is gradually varied from the dark gray clay of the uppermost of Mg Fm., to the silty clay of the downmost of Fh Fm. Rigid and compact white calcareous cement (**Figure 2G**) appears in the lower part (127–118 m) of the Fh Fm. In the middle part (118–18 m), light brown silty clay–silts and dark brown fine–medium sands appear alternately. Most sediments are massive, while scour-filling structures are common. Subangular granules are sparse in silts and sands. The fragments of *Corbicula* are visible at the top of the part. The top (18–0 m) of the Fh Fm. is composed mainly of silts and clay, whereas with the mixture of very fine loess, the sediments present mess and obscurity.

3.2 Sedimentary environments

Emphasis is placed on grain size, color, fossils, bed geometry, texture, and structures of the deposits to assess sedimentary environments comprehensively. Sedimentary systems are divided into fluvial, deltaic, and lacustrine environments on a sketchy description of the Taiyuan Basin. Each system is further subdivided to bear out its reasonability.

3.2.1 Fluvial environment

The fluvial environment consists of channel deposits and overbank deposits, which are components of meandering river on low gradient terrain (Miall, 1980; Miall, 1985; Reading, 2009). The channel deposits are dominated by coarse-grained sediments, which usually have a larger particle size than silt, while overbank deposits are primarily of fine-grained sediments

such as clay and silt. The channel and overbank sediments are typically treated as combination of binary structure (i.e., substratum and top stratum).

3.2.1.1 Channel deposits

The channel deposits consist of channel-fill and channel bar sediments. Channel-fill sediments are localized in the channel and divided into coarse-grained and fine-grained deposits (Middleton et al., 2003), depending on whether the channels are abandoned gradually or abruptly (Reading, 2009).

The coarse-grained channel deposits contain gravels lying on floors directly (also called lag deposits) and overlying sands. They are characterized by large grain size, thin layer, and lateral discontinuity. In the ZK01 core, the lag sediments are mainly distributed in the lower Xt Fm. They are composed mainly of sub-rounded pebbles, with sands overlying on the pebbles. Apparent erosive surfaces are common at the base of pebbles. The lag deposits are also seen in the upper Xt Fm. and in the base of Hy Fm. These deposits mark the position of abandoned channels.

The fine-grained channel deposits consist of silt and clay that are deposited in oxbow lakes. As channels are abandoned due to neck cutoff, they would provide relatively enclosed space for still water (Fisk, 1947), leading to the accumulation of overbank fines in oxbow lakes with an upward-fining sequence as the mud is laid on the top (Reading, 2009). Accordingly, the oxbow lake sediments in the Xt Fm. are hardly distinguished from the flood plain sediments in the core.

Channel-bar, also known as point bar, is the sediments of river migration on the floodplain. They usually emerge with the lag deposits, constituting upward-fining sequences. The sand bars from the core are mainly fine–coarse sand of normal grading, with relatively low textural maturity. However, distinct trough cross-beddings and planar cross-beddings are absent, which may be attributed to the limitation of the borehole core. The thickness of the sand bar horizon is usually less than 1 m. Brownish red is the dominant tone of the sands, reflecting subaerial deposition under oxidation. The sand bars deposits are mainly in the lower part of Xt Fm. and Fh Fm. Unlike the widespread development in Xt Fm., sand bars deposits are infrequent in Fh Fm., indicating a farther depositional site from the active river.

3.2.1.2 Overbank deposits

The overbank deposits are sediments out of channels, including nature levees, crevasse splays, and floodplain sediments. Generally, deposits of overbank are much finer than that of channels. Besides, the recognition of paleosols is also helpful to distinguish these deposits in overbank sediments (Kraus, 1999).

The nature levees are featured by intercalated thin muds and fine sands (Farrell, 1987; Collison et al., 2006). They are formed during major floods as the suspended materials spill out of the channel and then accumulate on the banks (Jordan and Pryor, 1992). In the lower part of the Xt Fm., the levee deposits are uncommon and very thin, probably eroded by overlying channel deposits. It is noteworthy that a suspected paleosol layer of the levee in the lower part of the Xt Fm. demonstrates a subaerial

exposure environment. In the Fh Fm., the nature levees are characterized by thin mud interfingering with thin silt.

Commonly, the channel is confined by bilateral levees. However, floodwaters may overtop the levees and destroy the banks. In this case, the flood deposits extend down the levees and spread onto the floodplain as crevasse splays (Jordan and Pryor, 1992; Reading, 2009). The crevasse splay deposits are dominantly of silt and fine sand, and coarse sand at the base. They usually lie between silt and mud layers with scour-filling structures at the base in the upper Xt Fm. The existence of mud clasts further exemplifies the scouring on levees or floodplain deposits. The crevasse splay deposits are also visible in the upper part of Xb Fm. and Fh Fm.

The floodplain deposits are the finest-grained fractions, which are typically of clay and silt in the non-lacustrine settings. Bioturbation and paleosols are well developed on account of slow sediment accumulation rates (Middleton et al., 2003). The floodplain deposits achieve a dominant position in the upper Xt Fm. and the Fh Fm. Muds of the floodplain encase sand bodies of crevasse splays and channels. Small and multichannel floodplain streams, instead of large-scale meandering channels represented by large tabular cross-bedding sands, dominate the floodplain construction in the east Taiyuan Basin. The light brick-red silts and clay in the upper Xt Fm. indicate an oxidized exposure environment. In addition, the paleosols further prove the exposure environment just as what the color has stated.

3.2.2 Deltaic environment

The deltaic environment is the product of interactions of various environments, such as rivers, lakes, and alluvial fans (Moore and Asquith, 1971). It is divided into delta plain, delta front, and prodelta subenvironments. However, it is difficult to distinguish the microfacies in the core so that the subenvironments are depicted concisely. The delta deposits are usually fine-upward or coarsening-upward sequences, depending on transgression or regression of the lake.

3.2.2.1 Delta plain deposits

The delta plain deposits are similar to that of the river because the delta plain is in the transition zone between river and lake. Hence, the recognition features of a delta can follow that of a river. Nevertheless, deposits of delta plain are finer in grain size and smaller in scale, which are mainly composed of sands, silts, and muds. The black organic-rich beds in the Xb Fm. are interpreted as swamp environments in interdistributary bays along the edge of the delta plain (Fielding, 1984; Nichols, 2009). Besides, the calcareous duricrusts are arrested in unconsolidated sediments. They present as highly resistant surfaces that develop under subaerial weathering environments over long periods in semi-arid climate (Nichols, 2009), emerging on channel or delta (Carlisle, 1983). They jointly constitute the delta plain environment with abundant erosive structures, paleosols, and fining-upward sands in strata.

3.2.2.2 Delta front deposits

The deposits in the delta front environment are strongly affected by wave and tide action (Nichols, 2009).

Consequently, the wavy bedding and tidal rhythmite in the Xb Fm (Figure 2H) consisting of intercalation of thin silts and muds are the significant identification markers. Broken shells are also present, which represent high-energy environments, the beach pounding by waves, for instance (Jones, 2014). Although the channels are not developed as in the delta plain environment, the subaqueous channels are still visible in the form of finer materials and their erosive undersurfaces. Contorted beds from the upper part of the Hy Fm (Figure 2I) occur on the delta front surface when subjected to vibration such as earthquake, since the high slope angle of the delta front provides such an unstable sedimentary condition (Mills, 1983).

3.2.2.3 Prodelta deposits

The prodelta deposits are mainly suspended sediment traveling away from the delta front (Nichols, 2009). Hence, it is similar to the lacustrine muds, both featured by massive and horizontal beddings (e.g., lower part of the Mg Fm.). Nevertheless, the prodelta deposits have more silts and fewer clays than that of the lake (e.g., Xt Fm. and Xb Fm.).

In conclusion, the delta deposits from the borehole core are generally fine grained, distinct from fan delta or braided river delta (Schomacker et al., 2010; Gobo et al., 2015; Lin et al., 2018). We attribute it to the low energy of the meandering river delta. On the other hand, the absence of steeply dipping foreset beds exemplifies a gentle slope basin margin of a finer-grained fluvial delta rather than a typical Gilbert-type coarse-grained delta. Furthermore, it is also in accordance with the tectonic setting of the half-graben basin, as the drill hole is on the inactive side of the basin, which has a low gradient slope and subsidence rate (Allen and Allen, 2013).

3.2.3 Lacustrine environment

3.2.3.1 Lacustrine deposits

The lacustrine deposits consist of interlaminated muds, silts, and very fine sands. The content of coarser materials depends on their depth in the lake basin. In the drill core, thick massive muds are interpreted as the lacustrine deposits, while the thinly interbedded silts with erosive bottoms as subaqueous channel deposits or sandy turbidity current deposits that went deep into the lake during floods or seismic activity (Mills, 1983). The lacustrine deposits are mainly in the lower part of Xb Fm. and Mg Fm. Rhythmities are the most characteristic sedimentary structures of deep lacustrine facies composed of pale carbonate-rich and dark organic-rich stratifications (Figure 2J). The interlayers of carbonates and organic matters reveal a characteristic facies of deep basin (Eugster and Kelts, 1983). However, lower Mg Fm. deposits containing more erosive structures and shell fragments are more likely to be a shallower lake environment. Indeed, they even failed to be distinguished from the prodelta deposits.

According to the distributions of the rhythmities, two great-lake periods can be distinguished in the lower Xb Fm. and lower Mg Fm., respectively (Figure 3). The lacustrine deposits in the Xb Fm. demonstrate a deep lake environment. They are swiftly

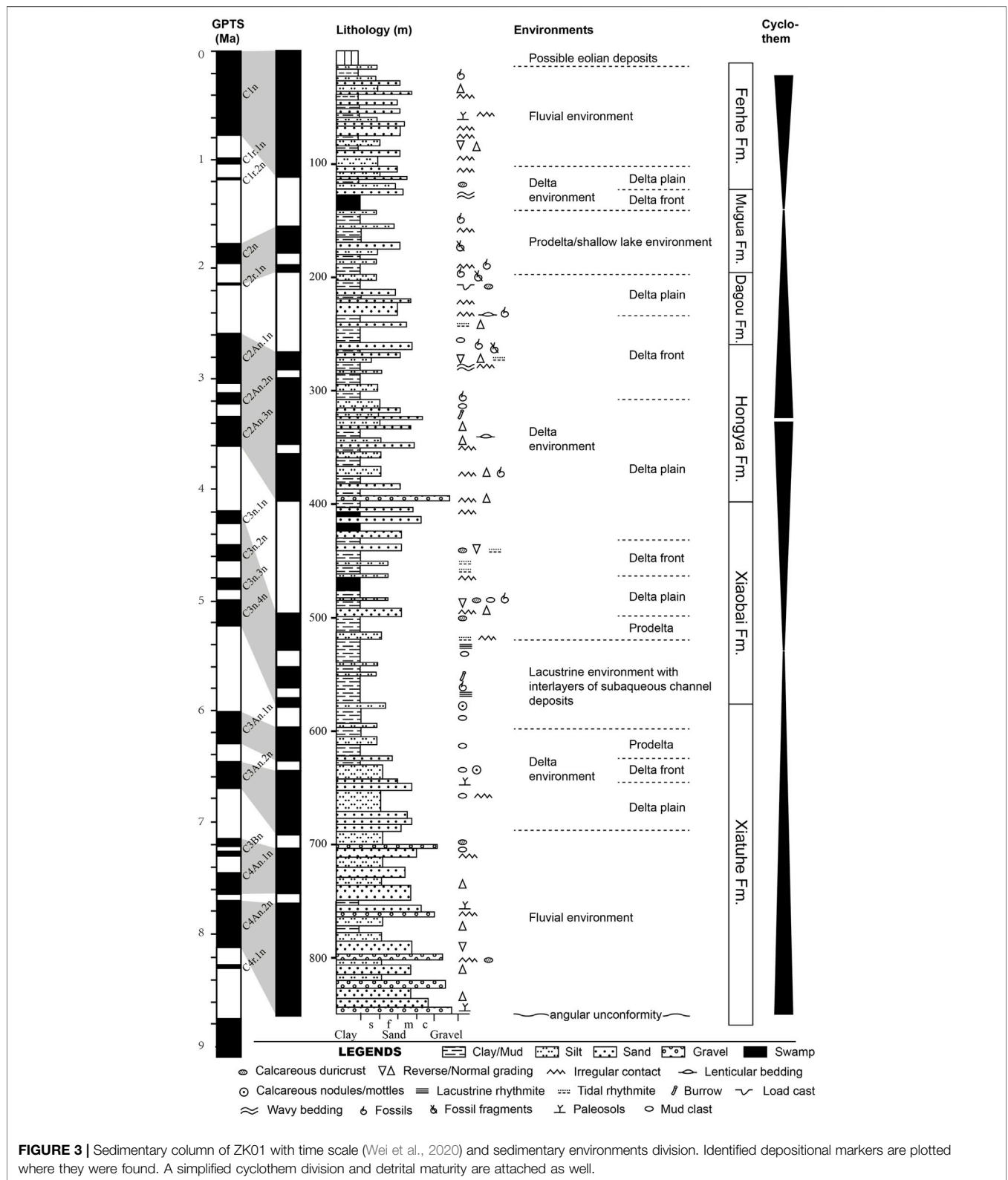


FIGURE 3 | Sedimentary column of ZK01 with time scale (Wei et al., 2020) and sedimentary environments division. Identified depositional markers are plotted where they were found. A simplified cyclothem division and detrital maturity are attached as well.

shifted from brown silts–clays to whitish and dark gray muds, which indicate sudden subsidence of the Taiyuan Basin. The vertical changes of the lake level can be dramatic and rapid on

account of a steeper lake basin margin in such a rift-basin setting (Reading, 2009). Beside of the lake level, facies changes are synchronous.

4 DRILL CORE GEOCHEMISTRY

A total of 34 bulk samples were collected for the analysis of major and trace element concentrations from the drill core of ZK01. Most samples came from clay and silts in the fluvial-lacustrine deposits, seldom from sand, and no samples were collected in conglomeratic units. Geochemical analysis was carried out at Taiyuan Mineral Resources Supervision and Testing Center of Ministry of Land and Resources. Samples were powdered to less than 200 mesh in an agate mortar and then placed in an oven at 105°C for drying for 12 h. Major oxides were tested by XRF analysis and had the analytical precision of 1%–2%. Trace element analyses were conducted on Agilent 7700e ICP-MS. Sample powder (50 mg) was disposed of to make the final solution for ICP-MS testing. Detailed procedures (see Cullen et al., 2001) are omitted here. The analytical precision is better than 5%.

4.1 Major elements concentration

The major element contents of the samples are listed in the **Supplementary Table S1**. The variations of element compositions along the depth of the drill core are plotted in **Supplementary Figure S1**. The SiO₂ content varies between 16.36 and 84.08 wt%, with an average of 57.92 wt%. Al₂O₃ content varies from 4.40 to 18.31 wt% with an average of 12.80. Compared with the upper continental crust (UCC) average content (Taylor and McLennan, 1985) (dash line in **Supplementary Figure S1**), SiO₂, Al₂O₃, Fe₂O₃, and TiO₂ are apparently lower in content at a depth of about 120–180 m (i.e., Mg Fm.) and 480–580 m (i.e., the lower part of Xb Fm.). Considerable loss appears at around 570 m. While it is exactly reverse for MgO and CaO, which are prominently enriched at the lower part of Xb Fm. All samples for Na₂O are depleted. SiO₂, Al₂O₃, Fe₂O₃, and TiO₂ content have similar curves in shape, indicating a statistically significant correlation ($r = 0.45$ to 0.96 ; $n = 34$; **Supplementary Table S2**). CaO and MgO content ($r = 0.47$; $n = 34$) have similar curves in shape but exactly opposite to that of the SiO₂ series ($r = -0.5$ to -0.93 , and -0.19 to -0.70 , respectively; $n = 34$), marking complementary features with the SiO₂ series. In addition to the two complementary series, no distinct changing trends are displayed between MnO, Na₂O, and P₂O₅.

4.2 Trace elements concentration

Trace element concentrations of the samples are listed in the **Supplementary Table S1**. The normalized patterns of each strata formation's average trace element concentrations against average UCC values are shown in **Supplementary Figure S2**. In comparison with the UCC, the samples are generally low in Zr, Ni, Cr, V, Sc, Co, and Mo. On the contrary, Rb, Th, Pb, Zn, La, and Ce are enriched with a few exceptions. Zn is highly consistent with most trace elements other than Mo, Ba, and U ($r = 72$ to 0.96 ; $n = 34$) (**Supplementary Table S3**). In comparison, Zr and Mo are little related to other trace elements ($r = -0.56$ to 0.52 and $r = -0.35$ to 0.33 , respectively; $n = 34$). Samples from Mg Fm. manifest that the average content is depleted in most trace

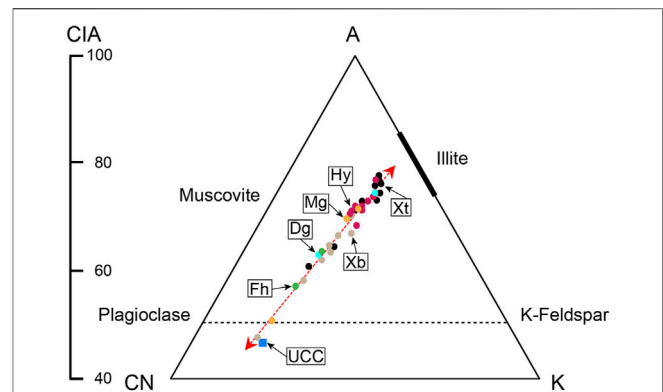


FIGURE 4 | The proportion of Al₂O₃–(CaO* + Na₂O)–K₂O–A–CN–K ternary plot and CIA index for the sand samples (after Nesbitt and Young, 1982 and Fedo et al., 1995).

elements. Nb, La, Ce, and Y of all samples plot a concentrated distribution, while the others exhibit a wide variation.

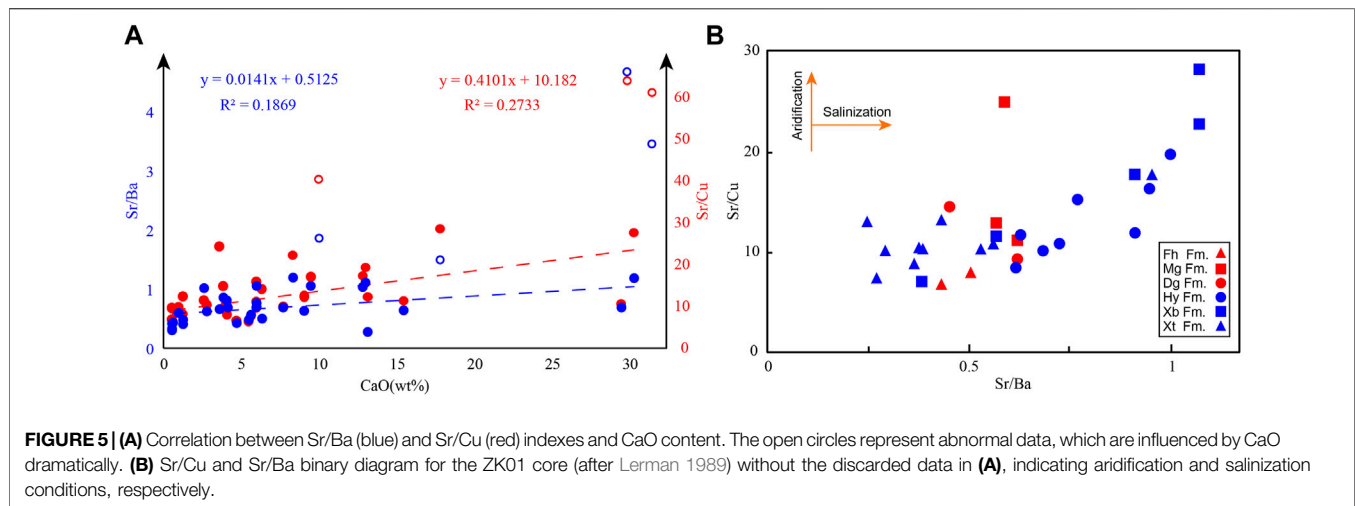
5 DISCUSSION

5.1 Paleoenvironment condition

5.1.1 Paleoweathering condition

The chemical index of alteration, namely, CIA (Nesbitt and Young, 1982), which reflects the ratio of immobile alumina to mobile alkalis, is widely used to measure the degree of weathering (Gallet et al., 1998; Tao et al., 2014; Wang et al., 2018; Armstrong-Altrin et al., 2019). The CIA values can be calculated by the formula $[\text{Al}_2\text{O}_3/(\text{Al}_2\text{O}_3 + \text{CaO}^* + \text{Na}_2\text{O} + \text{K}_2\text{O})] \times 100$, using molecular proportions. CaO* herein is the amount of CaO in silicates alone, ensuring inorganic carbon derivation. The CaO content was calculated according to Martinez et al. (2010). High CIA values reflect the removal of labile cations relative to stable residual constituents during weathering (Nesbitt and Young, 1982). Conversely, low CIA values indicate the near absence of chemical alteration, and consequently might reflect cool and/or arid conditions. In this work, CIA values of all samples range from 48 to 78 with an average of 68 (**Supplementary Table S1**), indicating a low to moderate degree of chemical weathering of the source area.

The proportion of Al₂O₃–(CaO* + Na₂O)–K₂O can also be plotted as the A–CN–K ternary diagram (Fedo et al., 1995) (**Figure 4**). In the A–CN–K plot, most samples plot well above the plagioclase–K–feldspar join line (black dashed line), indicating that chemical weathering, rather than abrasion, has primarily affected bedrock by destroying feldspars (Nesbitt and Young, 1996). The samples are clustered toward illite, signifying the removal of Na₂O and CaO from the bulk composition due to chemical weathering, and the increase of illite minerals. Each Xb Fm. and Mg Fm. contains one sample located on the feldspar join line and near UCC square, respectively, indicating slightly weathered products. However, the Xt Fm. and Hy Fm. samples are closer to the illite end, implying more exhaustive weathering processes.



5.1.2 Paleoclimate condition

The content and distribution patterns of various elements show differences in different climate conditions. In humid climates, lake levels are high, and water is diluted, with higher contents of Fe, Al, Ba, and Zn in sediments, while in arid climates, the water evaporates, and the aqueous medium becomes strong alkaline, with abundant Na, Ca, Mg, Cu, Sr, and Mn precipitates over the underlying sediment (Meng et al., 2012; Tian and Zhang, 2016). We use the ratio of Sr, Ba, and Cu instead of the value of a single element as the index to analyze paleoclimate, which can minimize the effect of source rock, highlighting the information obtained in sedimentation.

Sr/Ba ratio reflects lake water's concentration degree and, ultimately, the water salinity (Chivas et al., 1985; Sun, 1997; Fu et al., 2016). The ratio of Sr and Cu can be a proxy of aridification (Lerman, 1989; Meng et al., 2012). However, the carbonate-hosted Sr may alter the Sr/Ba and Sr/Cu signals from clay fraction (wei et al., 2018; Wei and Algeo, 2020). Hence, we inspected the correlation between the values of indexes and the content of CaO (Figure 5A). We found that only four samples (open circles) had the abnormal Sr/Ba and Sr/Cu values that were affected by CaO obviously. After removing these samples, the rest of the samples (solid circles) showed weak correlation between the indexes and CaO. Thus, we believe that it is reasonable to discuss the salinity using Sr/Ba and Sr/Cu index after we discarded the abnormal samples. Sr/Cu and Sr/Ba show a linear relationship in Figure 5B, indicating a good overall evaluation of the paleoclimate. It is worth noting that the Xt Fm. is plotted as relative humid environments, while Xb Fm. is in arid condition. The result demonstrates that the incipient sediments from the fluvial system were deposited under a humid environment, whereas the following lake was developed in arid environments.

The results are not conducive to the rapid development of the lake of the Xb Fm. This indicates that climate change may not be the primary driver in the transition from the fluvial to lacustrine system in Taiyuan Basin. Subsidence derived from tectonic movement provides accommodation and blocks the streams

flowing out the basin, which probably builds closer ties with the expansion of the lake.

5.2 Sedimentary environments and controlling factors

5.2.1 Evolution of the sedimentary environments

It is divided into three sections for the correlation of the strata in different boreholes, which are the bottom section of fluvial sediments, the middle section of lacustrine and deltaic sediments, and the top section of fluvial sediments, respectively. Coarse-grained fluvial sediments at the bottom of cores ZK01, J7, and T2, represent the response of the rapid subsidence process in the initial basin faulting stage. As the gravel convert to fine sand and mud upward, the grain size of sediments decrease sharply in the middle section. Because there are almost no thick layers of sand and gravel except for the top and bottom of the boreholes, and scarce typical fluvial beddings, the middle sections of the cores J7, J2, and T2 are mainly of lacustrine and deltaic sediments. Thereinto, there are five periods of lacustrine deposits in cores J2 and J7, twice lacustrine deposits in core ZK01, and only one lacustrine deposits in core T2. It shows obvious regional characteristic. The lacustrine deposits are embedded by the deltaic sediments reflecting the shrinkage of the lakes. Reappearance of thick sand and gravel in the top section of cores represents the run-through of the Fen River. Furthermore, the dramatic decrease of the thickness and amount of mud also confirms the disappearance of the standing water environment. This feature can be observed in the upper section of all four cores, showing spatial comparability.

The sediments of basal alluvial facies converted upward to delta facies with grain size sharply decreased, reflecting the weakening of the tectonic movement. Then, the stable stage was presented by the first transgression of J7 and J2. However, the transgression event lasted for only a short time. It was characterized by thin lacustrine deposition, inconsistent with the deep lacustrine deposition in the lower part of core ZK01 in the NE basin margin. Accordingly, we believe that cores J7 and

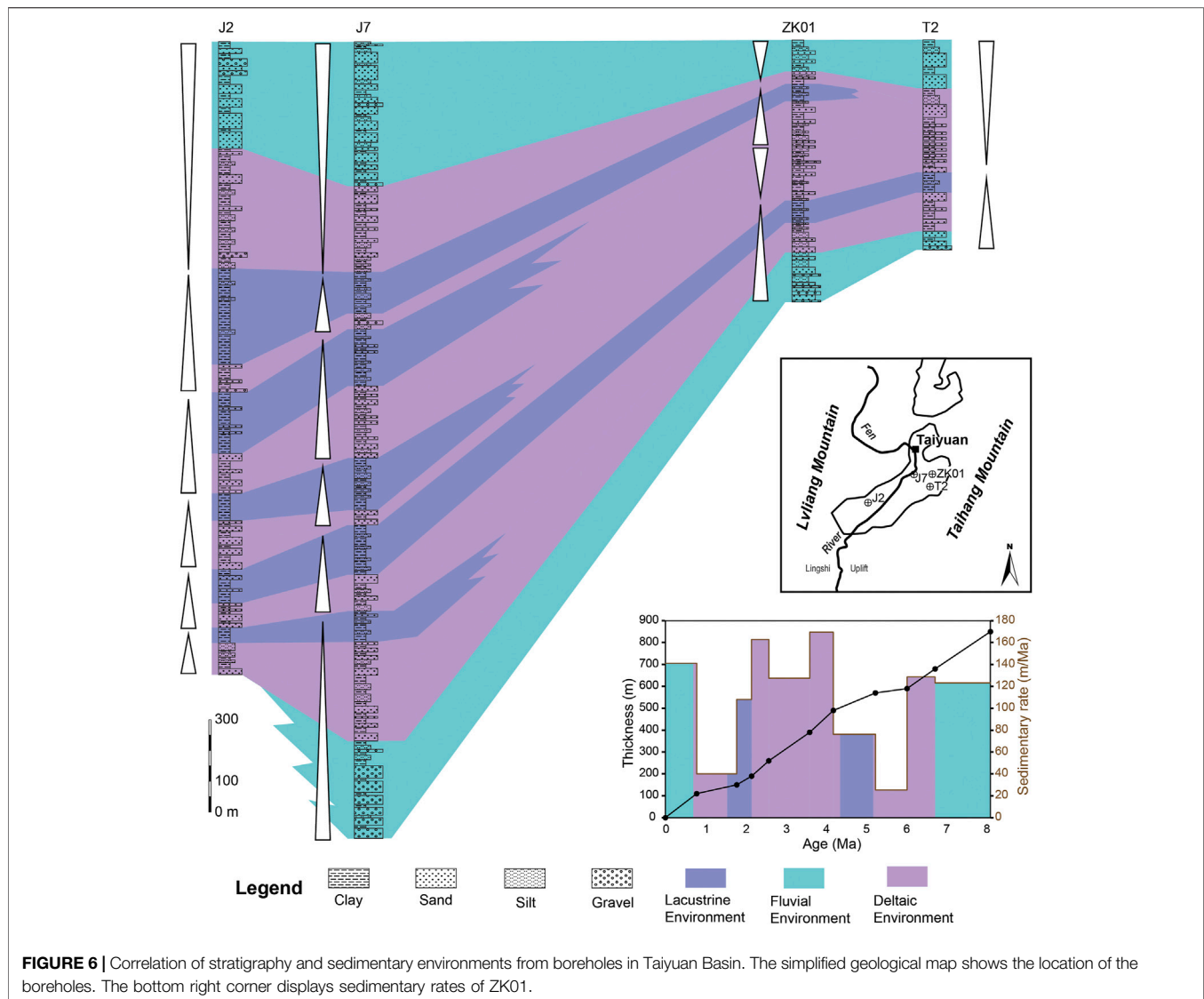


FIGURE 6 | Correlation of stratigraphy and sedimentary environments from boreholes in Taiyuan Basin. The simplified geological map shows the location of the boreholes. The bottom right corner displays sedimentary rates of ZK01.

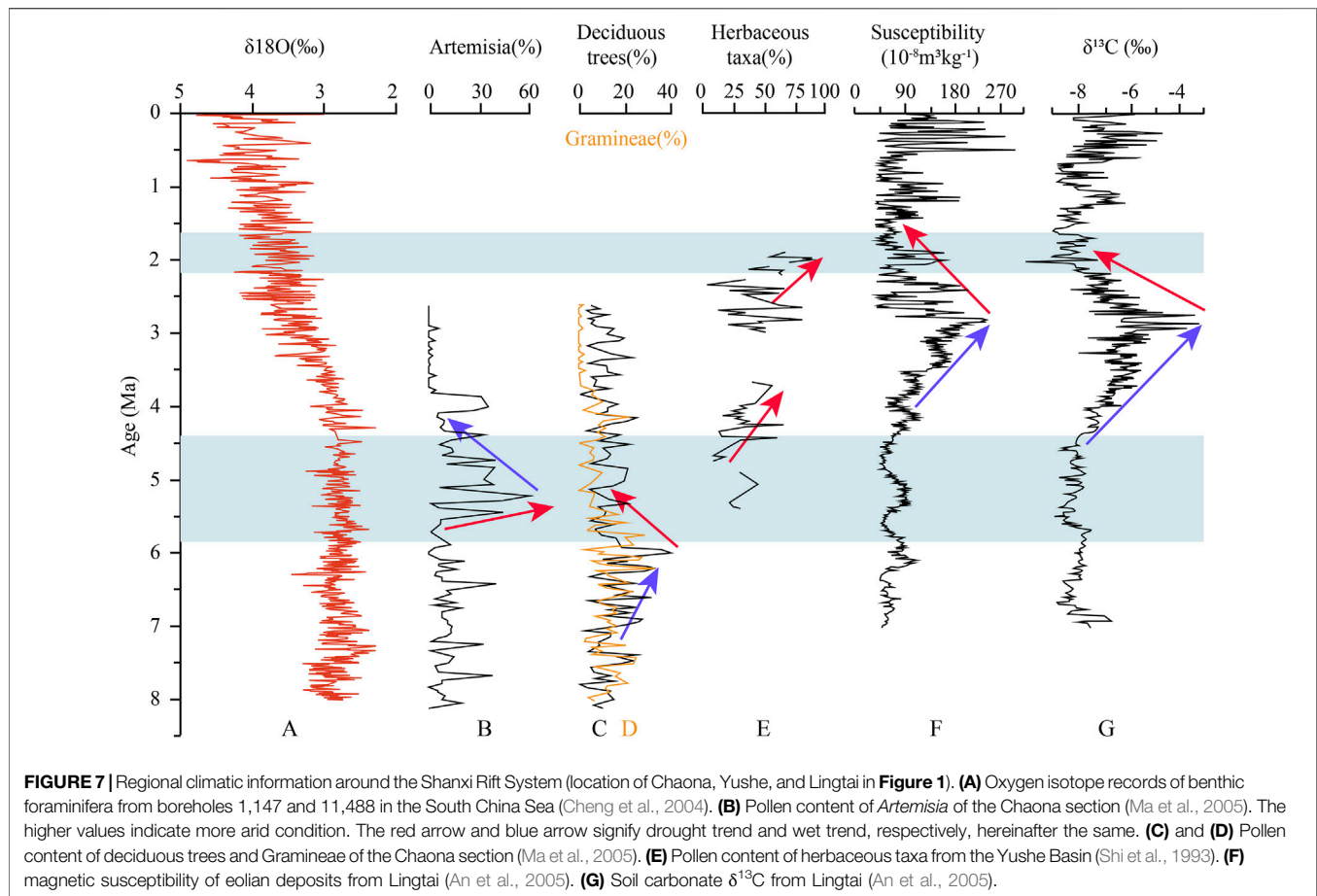
J2 experienced a small range of lake transgression, which failed to reach the positions of ZK01 and T2.

After the first transgression in J7 and J2, the following coarse-grained delta deposits advanced rapidly along the steep slope of the basin margin, capping the underlying fine-grained lacustrine sediments. Afterward, the accommodation was generated, contributing to the transgression during the subsequent tectonic quiescence. This transgression may be linked to the first transgression in cores ZK01 and T2. In ZK01, abrupt transition of sedimentary environments and relatively large deposition rate (Figure 6) exemplify accelerated lake expansion at ~5.2 Ma. Thereby, a lake covering the entire Taiyuan Basin formed during 5.2–6 Ma.

The third and fourth transgressions in J7 and J2 show a considerable thickness of lacustrine deposition. However, after the first lacustrine transgression, ZK01 was dominated by the interaction of delta plain and delta front deposits until ~2.2 Ma, and stable lacustrine deposits were no longer developed.

Furthermore, the second transgression of ZK01, which started at ~2.2 Ma, lasted for a short time and soon transformed into delta deposits and fluvial deposits. Therefore, it is difficult to compare the third and fourth transgression of cores J7 and J2 with the second transgression of ZK01. In the east of the basin, the principal manifestation is only a fluctuation of deepening and shallowing of the water body in the delta environment.

The fifth transgression of J7 and J2 was the last typical transgression event of these two boreholes. Thereinto, core J2 contains 300 m of lacustrine deposits, signifying a long time and large-scale transgression process. Hence, it is comparable to the second transgression of core ZK01. However, the shore-shallow lake sediments of core ZK01 are thin and insignificant with the pro-delta sedimentary characteristics. Moreover, corresponding transgression sediments are absent in core T2. It indicates that the position of T2 is beyond the reach of this transgression, and the west side of the basin has a larger subsidence amplitude than the east.



After that, neither the cores developed typical lacustrine deposits. It shows that the Taiyuan Basin lakes were gradually shrinking. After 0.6 Ma of core ZK01, the delta environment changed into a fluvial environment, and the lake shrank dramatically until it was completely emptied. Thus, there were five large-scale lake transgressions totally in Taiyuan Basin during the late Cenozoic. Two of them reached the basin's eastern edge, forming the super-large lake that almost covered the whole Taiyuan Basin. These two super-large lake periods are late Miocene to early Pliocene (~5.8–~4.4 Ma) and early stage of early Pleistocene (~2.2–1.6 Ma), respectively.

5.2.2 Controlling factors of lake evolution

In a continental basin, the internally sedimentary architecture is most likely under the control of tectonism and climatic variations (Allen and Allen, 2013; Birgenheier et al., 2019). Specifically, lakes are the products of active tectonic and moister climates (Reading, 2009). Here, we attempt to discuss the main controlling factors of lacustrine evolution in the Taiyuan Basin.

From a regional perspective, the East Asia has experienced an overall drying and cooling process (Guo et al., 2002; Deng et al., 2006; Cheng et al., 2004, **Figure 7A**) since the late Miocene, on account of sea ice expansion in the Northern Hemisphere (Jansen and Sjolholm, 1991) and uplift of the Tibetan Plateau (Manabe and Broccoli, 1990; An et al., 2001). Specifically, the Shanxi Rift

System is located in the eastern margin of the present Loess Plateau. According to the magnetic grain-size records (Nie et al., 2013), and pollen records of *Artemisia*, deciduous trees and Gramineae (Ma et al., 2005) of the Chaona section, the Loess Plateau is not unusually humid during ~5.8–4.4 Ma, and even has an aridification trend (Ma et al., 2005, **Figures 7B–D**). Although some results depict differing views that the summer precipitation was increased in this period due to enhanced summer monsoon (Wu et al., 2006; Chen et al., 2007; Li Jianxing et al., 2015), simulated summer precipitation for late Miocene and Pliocene presents its difference less than 100 mm/year (Ao et al., 2021) in the Taiyuan Basin. This cannot make a decisive impact on sedimentary environments of the Taiyuan Basin because the most increased precipitation is blocked by the Taihang Mountain. From 2.2 to 1.6 Ma, it is the period of strengthening monsoon with frequent and violent climate fluctuations. The pollen proportion of the herbaceous taxa from the Yushe Basin (**Figure 7E**, Shi et al., 1993), and magnetic susceptibility (**Figure 7F**) and soil carbonate $\delta^{13}\text{C}$ (**Figure 7G**) from Lingtai (An et al., 2005) all show a remarkable aridification tendency. It is consistent with what the Sr/Cu index presents and unfavorable for the expansion of the lake. Consequently, climate change is evidently not a direct factor in forming the two super-large lake periods.

Results of depositional environment and depositional cycle division of the drill cores reveal a close relationship between location (distance from active fault) and evolution of the drill holes (Figure 6). Cores J7 and J2 lie in the west of the basin, ahead of the steep slope with intense fault depression, developing at least five transgressions. In comparison, ZK01 and T2 are on the gentle slope of the east side with weak subsidence, involving simply two events. Hence, the Jiaocheng Fault activity can be effectively preserved by coarse-grained sediments. The Taigu Fault, however, can be recorded by sediments only during significant events. The close relevance between the sedimentary styles and their tectonic position reflects that tectonism rather than climate variations should mainly control the environmental changes of the Taiyuan Basin. Additionally, the first transgression coincides with the rapid uplift event of the Lvliang Mountain at about 5.7 Ma (Pan et al., 2018), and the second transgression corresponds to the change of stress regime of the rift from ca. 1.8 Ma (Shi et al., 2015). Therefore, the two transgressions represent two major tectonic events.

We speculate that the paleolakes originated from the backwater of the blocked paleorivers due to the differential uplift at the basin rim. At present, the Lingshi Uplift has an average elevation of 1,100 m in the northern mountains area on both sides of Fenhe Valley, much higher than the southern basin with a height of 750 m. In spite lacking the uplift rate, this fact indicates that the Lingshi Uplift blocked the drainage system from entering the Linfen Basin. As the lake in Taiyuan Basin reached its maximum flooding surface, the water overflowed the Lingshi Uplift and spilled southward to the Linfen Basin. Meanwhile, the spillover caused headward erosion at the boundary of Lingshi Uplift and Linfen Basin. When the river incised to the same height as the basin's surface, the ancient lake in Taiyuan Basin was gradually evacuated, and the Fen River recurred and flowed through the whole Taiyuan Basin eventually.

6 CONCLUSION

In the Taiyuan Basin of the Shanxi Rift System, thick deposits accumulated at ca. 8.1 Ma, recording the rift development. Sedimentary environment evolution indicates that two basin-wide lacustrine transgression events occurred at ca. 5.8–4.4 and ca. 2.2–1.6 Ma, respectively. In addition, the parent rock lithology changed significantly when the coarse clastic sediments of the syn-rift phase converted to the lacustrine sediments at ca. 5.8 Ma. It reveals two different depositional

systems before and after 5.8 Ma. We believe that these two transgressions are a response to the rapid subsidence of the basin and are controlled mainly by tectonism rather than climate variation. Hence, the Taiyuan Basin experienced at least two tectonic events at ca. 5.8 and 2.2 Ma.

DATA AVAILABILITY STATEMENT

The original contributions presented in the study are included in the article/Supplementary Material. Further inquiries can be directed to the corresponding author.

AUTHOR CONTRIBUTIONS

QZ did the field work, data processing, and wrote the manuscript. HH and RW contributed to the conception and provided funding for the study. HH reviewed and edited the manuscript. All authors contributed to the manuscript revision and discussion, and approved the submitted version.

FUNDING

This research was supported by the National Science Foundation of China (41872213, U1939201, 41702221, and 41602206) and Geological Prospecting Fund Project of Shanxi Bureau of National Territory Resources (HXCT01-2018F005). Shanxi Taiyuan Continental Rift Dynamics National Observation and Research Station (NORSTY20-04).

ACKNOWLEDGMENTS

We are grateful to Pengsheng Yang and Xiao Hu for their assistance in core logging and sample collection. We are particularly grateful to Qinmian Xu and Chengfa Lin for their helpful discussions.

SUPPLEMENTARY MATERIAL

The Supplementary Material for this article can be found online at: <https://www.frontiersin.org/articles/10.3389/feart.2022.833585/full#supplementary-material>

REFERENCES

- Allen, J. P., Fielding, C. R., Rygel, M. C., and Gibling, M. R. (2013). Deconvolving Signals of Tectonic and Climatic Controls from Continental Basins: An Example from the Late Paleozoic Cumberland Basin, Atlantic Canada. *J. Sediment. Res.* 83, 847–872. doi:10.2110/jsr.2013.58
- Allen, P. A., and Allen, J. R. (2013). *Basin Analysis: Principles and Application to Petroleum Play Assessment*. John Wiley & Sons.
- An, Z., Huang, Y., Liu, W., Guo, Z., Steven, C., Li, L., et al. (2005). Multiple Expansions of C4 Plant Biomass in East Asia since 7 Ma Coupled with Strengthened Monsoon Circulation. *Geology* 33 (9), 705–708.
- Ao, H., Rohling, E. J., Zhang, R., Roberts, A. P., Holbourn, A. E., Ladant, J.-B., et al. (2021). Global Warming-Induced Asian Hydrological Climate Transition across the Miocene-Pliocene Boundary. *Nat. Commun.* 12 (1), 6935. doi:10.1038/s41467-021-27054-5
- Armstrong-Altrin, J. S., Botello, A. V., Villanueva, S. F., and Soto, L. A. (2019). Geochemistry of Surface Sediments from the north Western Gulf of Mexico: Implications for Provenance and Heavy Metal Contamination. *Geol. Q.* 63, 522–538. doi:10.7306/gq.1484

- Armstrong-Altrin, J. S. (2009). Provenance of Sands from Cazon, Acapulco, and Bahía Kino Beaches, México. *Revista Mexicana de Ciencias Geológicas* 26, 764–782.
- Birgenheier, L. P., Berg, M. D. V., Plink-Björklund, P., Gall, R. D., Rosencrans, E., Rosenberg, M. J., et al. (2019). Climate Impact on Fluvial-Lake System Evolution, Eocene Green River Formation, Uinta Basin, Utah, USA. *GSA Bull.* 132, 562–587. doi:10.1130/b31808.1
- Boardman, E. L. (1989). Coal Measures (Namurian and Westphalian) Blackband Iron Formations: Fossil Bog Iron Ores. *Sedimentology* 36, 621–633. doi:10.1111/j.1365-3091.1989.tb02089.x
- Carlisle, D. (1983). “Concentration of Uranium and Vanadium in Calcretes and Gypcretes,” in *Residual Deposits; Surface Related Weathering Processes and Materials*. Editor R. C. L. Wilson (Geological Society of London Special Publications), 11, 185–195. doi:10.1144/gsl.sp.1983.011.01.19
- Chang, J., Qiu, N., Liu, S., Cai, C., Xu, Q., and Liu, N. (2018). Post-triassic Multiple Exhumation of the Taihang Mountains Revealed via Low-T Thermochronology: Implications for the Paleo-Geomorphologic Reconstruction of the North China Craton. *Gondwana Res.* 68, 34–49.
- Chen, G. (1987). On the Geotectonic Nature of the Fen-Wei Rift System. *Tectonophysics* 143, 217–223.
- Chen, X., Shi, W., Hu, J., and Dong, S. (2016). Sedimentation of the Pliocene–Pleistocene Chaizhuang Section in the central of Linfen Basin, North China and its Tectonic Significance. *J. Geomechanics* 22 (4), 984–994.
- Chen, X., Dong, S., Shi, W., Zuzza, A. V., Li, Z., Chen, P., et al. (2021). Magnetostratigraphic Ages of the Cenozoic Weihe and Shanxi Grabens in North China and Their Tectonic Implications. *Tectonophysics* 813, 1–12. doi:10.1016/j.tecto.2021.228914
- Chen, X., Fang, X., An, Z., Han, W., Wang, X., Bai, Y., et al. (2007). An 8.1Ma Calcite Record of Asian Summer Monsoon Evolution on the Chinese central Loess Plateau. *Sci. China Ser. D* 50, 392–403. doi:10.1007/s11430-007-0016-x
- Cheng, S. (1983). Discussion on the Capture of Qingshuihe River and Hutuohe River. *J. Hebei Sch. Geology* 2, 41–53.
- Cheng, X., Zhao, Q., Wang, J., Jian, Z., and Xia, P. (2004). Data Report: Stable Isotopes from Sites 1147 and 1148. *Proc. Odp, Sci. Results*. 184, 1–12. doi:10.2973/odp.proc.sr.184.223.2004
- Chivas, A. R., De Deckker, P., and Shelley, J. M. G. (1985). Strontium Content of Ostracods Indicates Lacustrine Palaeosalinity. *Nature* 316 (6025), 251–253. doi:10.1038/316251a0
- Clift, P. D., and Jonell, T. N. (2021). Himalayan-Tibetan Erosion Is Not the Cause of Neogene Global Cooling. *Geophys. Res. Lett.* 48, e2020GL087742. doi:10.1029/2020gl087742
- Clinkscales, C., and Kapp, P. (2019). Structural Style and Kinematics of the Taihang-Luliangshan Fold belt, North China: Implications for the Yanshanian Orogeny. *Lithosphere* 11, 767–783. doi:10.1130/11096.1
- Clinkscales, C., Kapp, P., Thomson, S., Wang, H., Laskowski, A., Orme, D. A., et al. (2021). Regional Exhumation and Tectonic History of the Shanxi Rift and Taihangshan, North China. *Tectonics* 40 (3), e2020TC006416. doi:10.1029/2020tc006416
- Clinkscales, C., Kapp, P., and Wang, H. (2020). Exhumation History of the north-central Shanxi Rift, North China, Revealed by Low-Temperature Thermochronology. *Earth Planet. Sci. Lett.* 536, 116146. doi:10.1016/j.epsl.2020.116146
- Collison, J. D., Mountney, N. P., and Thompson, D. B. (2006). *Sedimentary Structures*. Terra Publishing.
- Cullen, J. T., Paul Field, M., and Sherrell, R. M. (2001). Determination of Trace Elements in Filtered Suspended marine Particulate Material by Sector Field HR-ICP-MS. *J. Anal. Spectrom.* 16, 1307–1312. doi:10.1039/b104398f
- Deng, C., Shaw, J., Liu, Q., Pan, Y., and Zhu, R. (2006). Mineral Magnetic Variation of the Jingbian Loess/paleosol Sequence in the Northern Loess Plateau of China: Implications for Quaternary Development of Asian Aridification and Cooling. *Earth Planet. Sci. Lett.* 241, 248–259. doi:10.1016/j.epsl.2005.10.020
- Deng, C., Zhu, R., Zhang, R., Ao, H., and Pan, Y. (2007). Timing of the Nihewan Formation and Faunas. *Quat. Res.* 69, 77–90.
- Deng, Q., Chen, S., Min, W., Yang, G., and Reng, D. (1999). Discussion on Cenozoic Tectonics and Dynamics of the Ordos Block. *Int. J. Rock Mech. Min. Sci.* 5 (3), 13–21.
- Deng, Q., Wang, K., Wang, Y., Tang, H., Wu, Y., and Ding, M. (1973). Geological Conditions for Earthquakes in Down-Faulted Seismic Zone of Shanxi Uplift Region and Developmental Trend of Seismicity. *Scientia Geologica Sinica* 1, 37–74. (in Chinese with English abstract).
- Eugster, H. P., and Kelts, K. (1983). Lacustrine Chemical Sediments. In: *Chemical Sediments and Geomorphology* Ed. by A. S. Goudie and K. Pye, 321–368. Academic Press, London. 4.7.1.
- Farrell, K. M. (1987). “Sedimentology and Facies Architecture of Overbank Deposits of the Mississippi River, False River Region, Louisiana,” in *Recent Developments in Fluvial Sedimentology* (SEPM (Society of Sedimentary Geology) Special Publication), 39, 111–120. doi:10.2110/pec.87.39.0111
- Fedo, C. M., Wayne Nesbitt, H., and Young, G. M. (1995). Unraveling the Effects of Potassium Metasomatism in Sedimentary Rocks and Paleosols, with Implications for Paleoweathering Conditions and Provenance. *Geol* 23 (10), 921–924. doi:10.1130/0091-7613(1995)023<0921:uteopm>2.3.co;2
- Fielding, C. R. (1984). A Coal Depositional Model for the Durham Coal Measures of NE England. *J. Geol. Soc.* 141, 919–931. doi:10.1144/gsjgs.141.5.0919
- Fisk, H. N. (1947). *Fine-grained Alluvial Deposits and Their Effect on Mississippi River Activity*. Mississippi River Commission: Vicksburg.
- Fu, X., Wang, J., Chen, W., Feng, X., and Wang, D. (2016). Elemental Geochemistry of the Early Jurassic Black Shales in the Qiangtang Basin, Eastern Tethys: Constraints for Palaeoenvironment Conditions. *Geol. J.* 51, 443–454.
- Gallet, S., Jahn, B.-m., Van Vliet Lanoë, B., Dia, A., and Rossello, E. (1998). Loess Geochemistry and its Implications for Particle Origin and Composition of the Upper continental Crust. *Earth Planet. Sci. Lett.* 156, 157–172. doi:10.1016/s0012-821x(97)00218-5
- Gobo, K., Ghinassi, M., Nemeč, W., and Walsh, J. P. (2015). Gilbert-type Deltas Recording Short-Term Base-Level Changes: Delta-Brink Morphodynamics and Related Foreset Facies. *Sedimentology* 62, 1923–1949. doi:10.1111/sed.12212
- Guo, Z. T., Ruddiman, W. F., Hao, Q. Z., Wu, H. B., Qiao, Y. S., Zhu, R. X., et al. (2002). Onset of Asian Desertification by 22 Myr Ago Inferred from Loess Deposits in China. *Nature* 416, 159–163. doi:10.1038/416159a
- Hao, Q., and Guo, Z. (2004). Magnetostratigraphy of a Late Miocene-Pliocene Loess-Soil Sequence in the Western Loess Plateau in China. *Geophys. Res. Lett.* 31, 1–4. doi:10.1029/2003gl019392
- Haszeldine, R. S. (1984). Muddy Deltas in Freshwater Lakes, and Tectonism in the Upper Carboniferous Coalfield of NE England. *Sedimentology* 31, 811–822. doi:10.1111/j.1365-3091.1984.tb00888.x
- Heberer, B., Anzenbacher, T., Neubauer, F., Genser, J., Dong, Y., and Dunkl, I. (2014). Polyphase Exhumation in the Western Qinling Mountains, China: Rapid Early Cretaceous Cooling along a Lithospheric-Scale Tear Fault and Pulsed Cenozoic Uplift. *Tectonophysics* 617, 31–43. doi:10.1016/j.tecto.2014.01.011
- Hu, Z., Pan, B., Wang, J., Cao, B., and Gao, H. (2012). Fluvial Terrace Formation in the Eastern Fenwei Basin, China, during the Past 1.2Ma as a Combined Archive of Tectonics and Climate Change. *J. Asian Earth Sci.* 60, 235–245. doi:10.1016/j.jseas.2012.09.016
- Huang, Y., Wang, Q., Hao, M., and Zhou, S. (2018). Fault Slip Rates and Seismic Moment Deficits on Major Faults in Ordos Constrained by GPS Observation. *Sci. Rep.* 8, 16192–16199. doi:10.1038/s41598-018-34586-2
- Jansen, E., and Sjöholm, J. (1991). Reconstruction of Glaciation over the Past 6 Myr from Ice-Borne Deposits in the Norwegian Sea. *Nature* 349, 600–603. doi:10.1038/349600a0
- Jiang, W., Guo, H., Xie, X., Zhang, L., and Xu, J. (2012). *Report of 1: 50000 Active Fault Mapping of Jiaocheng Fault Zone in Shanxi*. Institute of Crustal Stress, China Earthquake Administration Publication.
- Jones, S. J. (2014). *Introducing Sedimentology*. Dunedin Academic Press Ltd.
- Jordan, D. W., and Pryor, W. A. (1992). Hierarchical Levels of Heterogeneity in a Mississippi River Meander belt and Application to Reservoir Systems. *AAPG Bull.* 76 (10), 1601–1624. doi:10.1306/bdff8a6a-1718-11d7-8645000102c1865d
- Kraus, M. J. (1999). Paleosols in Clastic Sedimentary Rocks: Their Geologic Applications. *Earth-Science Rev.* 47, 41–70. doi:10.1016/s0012-8252(99)00026-4
- Kusky, T. M., Windley, B. F., and Zhai, M.-G. (2007). “Tectonic Evolution of the North China Block: from Orogen to Craton to Orogen,” in *Mesozoic Sub-Continental Lithospheric Thinning under Eastern Asia*: *Geol.* Editors M. Zhai, B. F. Windley, T. M. Kusky, and Q. Meng (Geological Society, London: Special Publications Soc. London Special Publication), 280, 1–34. doi:10.1144/sp280.1

- Lerman, A. (1989). *Lakes, Chemistry, Geology, Physics*. Springer-Verlag Berlin Heidelberg GmbH.
- Li, B., Sørensen, M. B., and Atakan, K. (2015). Coulomb Stress Evolution in the Shanxi Rift System, North China, since 1303 Associated with Coseismic, post-seismic and Interseismic Deformation. *Geophys. J. Int.* 203, 1642–1664. doi:10.1093/gji/ggv384
- Li, J., Liu, C., Yue, L., and Wang, J. (2015). Apatite Fission Track Evidence for the Cenozoic Uplift of the Lüliang Mountains and a Discussion on the Uplift Mechanism. *Chin. Geol.* 42 (4), 960–972. (in Chinese with English abstract).
- Li, P., and Liang, Q. (1965). New Information on Channel Change of the Upstream of Hutuohe River and Mumahe River. *Geol. Rev.* 23 (3), 240–241.
- Lin, C., Liu, S., Zhuang, Q., and Steel, R. J. (2018). Sedimentation of Jurassic Fan-Delta Wedges in the Xiahuayuan Basin Reflecting Thrust-Fault Movements of the Western Yanshan Fold-And-Thrust Belt, China. *Sediment. Geology* 368, 24–43. doi:10.1016/j.sedgeo.2018.03.005
- Liu, J., Zhang, P., Lease, R. O., Zheng, D., Wan, J., Wang, W., et al. (2013). Eocene Onset and Late Miocene Acceleration of Cenozoic Intracontinental Extension in the North Qinling Range-Weihe Graben: Insights from Apatite Fission Track Thermochronology. *Tectonophysics* 584, 281–296. doi:10.1016/j.tecto.2012.01.025
- Liu, P., Deng, C., Li, S., Cai, S., Cheng, H., Baoyin, Y., et al. (2012). Magnetostratigraphic Dating of the Xiashagou Fauna and Implication for Sequencing the Mammalian Faunas in the Nihewan Basin, North China. *Palaeogeogr. Palaeoclimatol. Palaeoecol.* 315–316, 75–85. doi:10.1016/j.palaeo.2011.11.011
- Liu, S., and Zhang, G. (2005). Fundamental Ideas, Contents and Methods in Study of basin and Mountain Relationships. *Earth Sci. Front.* 12, 101–111. (in Chinese with English abstract).
- Ma, X., Deng, Q., Wang, Y., and Liu, H. (1982). Cenozoic Graben System in north China. *Z. Geomorph. N.F.* 42, 99–116.
- Ma, Y., Wu, F., Fang, X., Li, J., An, Z., and Wang, W. (2005). Pollen Record from Red clay Sequence in the central Loess Plateau between 8.10 and 2.60 Ma. *Chin.Sci.Bull.* 50 (19), 2234–2243. doi:10.1007/bf03182675
- Manabe, S., and Broccoli, A. J. (1990). Mountains and Arid Climates of Middle Latitudes. *Science* 247 (4939), 192–195. doi:10.1126/science.247.4939.192
- Martinez, N. C., Murray, R. W., Thunell, R. C., Peterson, L. C., Muller-Karger, F., Lorenzoni, L., et al. (2010). Local and Regional Geochemical Signatures of Surface Sediments from the Cariaco Basin and Orinoco Delta, Venezuela. *Venezuela. Geology* 38, 159–162. doi:10.1130/g30487.1
- Meng, Q., Liu, Z., Bruch, A. A., Liu, R., and Hu, F. (2012). Palaeoclimatic Evolution during Eocene and its Influence on Oil Shale Mineralisation, Fushun basin, China. *J. Asian Earth Sci.* 45, 95–105. doi:10.1016/j.jseae.2011.09.021
- Miall, A. D. (1985). Architectural-element Analysis: a New Method of Facies Analysis Applied to Fluvial Deposits. *Earth-Science Rev.* 22 (4), 261–308. doi:10.1016/0012-8252(85)90001-7
- Miall, A. D. (1980). Cyclicity and the Facies Model Concept in Fluvial Deposits. *Bull. Can. Petrol. Geol.* 28, 59–80.
- Middleton, G. V., Church, M. J., Coniglio, M., Hardie, L. A., and Longstaffe, F. J. (2003). *Encyclopedia of Sedimentary Rocks*. Dordrecht: Kluwer Academic Publishers, 286.
- Mills, P. C. (1983). Genesis and Diagnostic Value of Soft-Sediment Deformation Structures-A Review. *Sediment. Geology* 35 (2), 83–104. doi:10.1016/0037-0738(83)90046-5
- Moore, G. T., and Asquith, D. O. (1971). Delta: Term and Concept. *Geol. Soc. America Bull.* 82, 2563–2568. doi:10.1130/0016-7606(1971)82[2563:dtac]2.0.co;2
- Nesbitt, H. W., and Young, G. M. (1982). Early Proterozoic Climates and Plate Motions Inferred from Major Element Chemistry of Lutites. *Nature* 299, 715–717. doi:10.1038/299715a0
- Nesbitt, H., and Young, G. (1996). Petrogenesis of Sediments in the Absence of Chemical Weathering: Effects of Abrasion and Sorting on Bulk Composition and Mineralogy. *Sedimentology* 43, 341–358. doi:10.1046/j.1365-3091.1996.d01-12.x
- Nichols, G. (2009). *Sedimentology and Stratigraphy*. John Wiley & Sons.
- Nie, J., Song, Y., King, J. W., Zhang, R., and Fang, X. (2013). Six Million Years of Magnetic Grain-Size Records Reveal that Temperature and Precipitation Were Decoupled on the Chinese Loess Plateau during ~ 4.5-2.6 Ma. *Quat. Res.* 79 (3), 465–470. doi:10.1016/j.yqres.2013.01.002
- Pan, B., Burbank, D., Wang, Y., Wu, G., Li, J., and Guan, Q. (2003). A 900 k.Y. Record of Strath Terrace Formation during Glacial-Interglacial Transitions in Northwest China. *Geology* 31, 957–960. doi:10.1130/g19685.1
- Pan, F., Li, J., Xu, Y., Wingate, M. T. D., Yue, L., Li, Y., et al. (2018). Uplift of the Lüliang Mountains at Ca. 5.7 Ma: Insights from Provenance of the Neogene Eolian Red clay of the Eastern Chinese Loess Plateau. *Palaeogeogr. Palaeoclimatol. Palaeoecol.* 502, 63–73. doi:10.1016/j.palaeo.2018.04.024
- Peltzer, G., Tapponnier, P., Zhitao, Z., and Qin, X. Z. (1985). Neogene and Quaternary Faulting in and along the Qinling Shan. *Nature* 317, 500–505. doi:10.1038/317500a0
- Qing, J.-C., Ji, J.-Q., Wang, J.-D., Peng, Q.-L., Niu, X.-L., and Ge, Z.-H. (2008). Apatite Fission Track Study of Cenozoic Uplifting and Exhumation of Wutai Mountain, China. *Chin. J. Geophys.* 51, 256–264. (in Chinese with English abstract). doi:10.1002/cjg2.1217
- Reading, H. G. (2009). *Sedimentary Environments: Processes, Facies and Stratigraphy*. 3rd ed. John Wiley & Sons, 83–106.
- Schomacker, E. R., Kjemperud, A. V., Nystuen, J. P., and Jahren, J. S. (2010). Recognition and Significance of Sharp-Based Mouth-Bar Deposits in the Eocene Green River Formation, Uinta Basin, Utah. *Sedimentology* 57, 1069–1087. doi:10.1111/j.1365-3091.2009.01136.x
- Shanxi Bureau of Geology and Mineral Resources (SBGMR) (1989). *Regional Geology of Shanxi Province*. Beijing: Geological Publishing House.
- Shi, N., Cao, J., and Lars-König, K. (1993). Late Cenozoic Vegetational History and the Pliocene-Pleistocene Boundary in the Yushe Basin, S. E. Shanxi, China. *Grana* 32 (4-5), 260–271.
- Shi, W., Cen, M., Chen, L., Wang, Y., Chen, X., Li, J., et al. (2015). Evolution of the Late Cenozoic Tectonic Stress Regime in the Shanxi Rift, central North China Plate Inferred from New Fault Kinematic Analysis. *J. Asian Earth Sci.* 114, 54–72. doi:10.1016/j.jseae.2015.04.044
- Shi, W., Dong, S., and Hu, J. (2020). Neotectonics Around the Ordos Block, North China: A Review and New Insights. *Earth-Science Rev.* 200, 1–34. doi:10.1016/j.earscirev.2019.102969
- Singer, A. (1980). The Paleoclimatic Interpretation of clay Minerals in Soils and Weathering Profiles. *Earth-Science Rev.* 15, 303–326. doi:10.1016/0012-8252(80)90113-0
- Su, P., He, H., Tan, X., Liu, Y., Shi, F., and Kirby, E. (2021). Initiation and Evolution of the Shanxi Rift System in North China: Evidence from Low-Temperature Thermochronology in a Plate Reconstruction Framework. *Tectonics* 40 (3), e2020TC006298. doi:10.1029/2020tc006298
- Sun, J. (2005). Long-term Fluvial Archives in the Fen Wei Graben, central China, and Their Bearing on the Tectonic History of the India-Asia Collision System during the Quaternary. *Quat. Sci. Rev.* 24, 1279–1286. doi:10.1016/j.quascirev.2004.08.018
- Sun, Z. (1997). *Sedimentary Environment and Hydrocarbon Generation of Cenozoic saline Lacustrine in China*. Beijing: Petroleum Industry Press, 125–141.
- Tang, Z., Yang, S., Qiao, Q., Yin, F., Huang, B., and Ding, Z. (2016). A High-Resolution Geochemical Record from the Kuche Depression: Constraints on Early Miocene Uplift of South Tian Shan. *Palaeogeogr. Palaeoclimatol. Palaeoecol.* 446, 1–10. doi:10.1016/j.palaeo.2016.01.020
- Tao, H., Sun, S., Wang, Q., Yang, X., and Jiang, L. (2014). Petrography and Geochemistry of Lower Carboniferous Greywacke and Mudstones in Northeast Junggar, China: Implications for Provenance, Source Weathering, and Tectonic Setting. *J. Asian Earth Sci.* 87, 11–25. doi:10.1016/j.jseae.2014.02.007
- Tapponnier, P., Peltzer, G., and Armijo, R. (1986). On the Mechanics of the Collision between India and Asia. *Geol. Soc. Lond. Spec. Publications* 19 (1), 113–157. doi:10.1144/gsl.sp.1986.019.01.07
- Tapponnier, P., Peltzer, G., Le Dain, A. Y., Armijo, R., and Cobbold, P. (1982). Propagating Extrusion Tectonics in Asia: New Insights from Simple Experiments with Plasticine. *Geol.* 10 (12), 611–616. doi:10.1130/0091-7613(1982)10<611:petian>2.0.co;2
- Tapponnier, R., and Molnar, R. (1977). Active Faulting and Tectonics in China. *J. Geophys. Res.* 82 (B20), 2905–2930. doi:10.1029/jb082i020p02905
- Taylor, S. R., and McLennan, S. M. (1985). *The continental Crust: Its Composition and Evolution*. United States.

- The Research Group on Active Fault System around Ordos Massif, State Seismological Bureau (RGAFSO) (1988). *Active Fault System Around Ordos Massif*. Beijing: Seismological Press, 1–335.
- Tian, J., and Zhang, X. (2016). *Sedimentary Geochemistry*. Beijing: Geological Publishing House, 67.
- Wang, N., Yang, J., Xia, Z., Mo, D., Li, Y., and Pan, M. (1996). *Cenozoic Sedimentary and Tectonic Geomorphology of Shanxi Rift System*. Beijing: Science Press. (in Chinese).
- Wang, P., Huang, Z., Mi, N., Xu, M., Wang, L., Li, H., et al. (2014). Crustal Structure beneath the Weihe Graben in central China: Evidence for the Tectonic Regime Transformation in the Cenozoic. *J. Asian Earth Sci.* 81, 105–114. doi:10.1016/j.jseas.2013.11.010
- Wang, X., Wan, Z., Chen, C., and Chen, S. (2021). Geochemical Characteristics of Hydrocarbons in Core Sediments from the Southwest Sub-Basin of the South China Sea and its Implications for the Sedimentary Environment. *Front. Earth Sci.* 9 (317), 1–10. doi:10.3389/feart.2021.664959
- Wang, Z., Wang, J., Fu, X., Zhan, W., Armstrong-Altrin, J. S., Yu, F., et al. (2018). Geochemistry of the Upper Triassic Black Mudstones in the Qiangtang Basin, Tibet: Implications for Paleoenvironment, Provenance, and Tectonic Setting. *J. Asian Earth Sci.* 160, 118–135. doi:10.1016/j.jseas.2018.04.022
- Wei, R., Zhuang, Q., Yan, J., Wei, Y., Du, Y., and Fan, J. (2020). *Late Cenozoic Stratigraphic Division and Sedimentary Environment of Jinzhong Basin in Shanxi Province, with the Climate and lake Evolution since the Pre-qin Period*. Geology in China.
- Wei, W., and Algeo, T. J. (2020). Elemental Proxies for Paleosalinity Analysis of Ancient Shales and Mudrocks. *Geochimica et Cosmochimica Acta* 287, 341–366. doi:10.1016/j.gca.2019.06.034
- Wei, W., Algeo, T. J., Lu, Y., Lu, Y., Liu, H., Zhang, S., et al. (2018). Identifying marine Incursions into the Paleogene Bohai Bay Basin lake System in Northeastern China. *Int. J. Coal Geology*. 200, 1–17. doi:10.1016/j.coal.2018.10.001
- Weltje, G. J., and Von Eynatten, H. (2004). Quantitative Provenance Analysis of Sediments: Review and Outlook. *Sediment. Geology*. 171, 1–11. doi:10.1016/j.sedgeo.2004.05.007
- Willis, B. (1907). *Research in China, V. I, Part I*, 233–236.
- Wu, C. (1996). Palaeochannel and Paleodrainage Patterns in the North China Mountains. *Geographical Res.* 15, 33–41. (in Chinese with English abstract).
- Wu, N., Pei, Y., Lu, H., Guo, Z., Li, F., and Liu, T. (2006). Marked Ecological Shifts during 6.2–2.4 Ma Revealed by a Terrestrial Molluscan Record from the Chinese Red Clay Formation and Implication for Palaeoclimatic Evolution. *Palaeogeogr. Palaeoclimatol. Palaeoecol.* 233 (3), 287–299. doi:10.1016/j.palaeo.2005.10.006
- Xu, X., Ma, X., and Deng, Q. (1993). Neotectonic Activity along the Shanxi Rift System, China. *Tectonophysics* 219, 305–325. doi:10.1016/0040-1951(93)90180-r
- Xu, X., and Ma, X. (1992). Geodynamics of the Shanxi Rift System, China. *Tectonophysics* 208, 325–340. doi:10.1016/0040-1951(92)90353-8
- Xu, Y. (2012). *A Study on the Late Quaternary Faulting of the Huoshan Piedmont Fault Zone in the central Shanxi Faulted basin belt*. China Earthquake Administration: Institute of Geology. (in Chinese).
- Xu, Y., Yue, L., Li, J., Sun, L., Sun, B., Zhang, J., et al. (2009). An 11-Ma-Old Red clay Sequence on the Eastern Chinese Loess Plateau. *Palaeogeogr. Palaeoclimatol. Palaeoecol.* 284, 383–391. doi:10.1016/j.palaeo.2009.10.023
- Yan, J., Hu, J., Gong, W., Liu, X., Yin, Y., and Tan, C. (2020). Late Cenozoic Magnetostratigraphy of the Yuncheng Basin, central North China Craton and its Tectonic Implications. *Geol. J.* 55, 7415–7428. doi:10.1002/gj.3744
- Yin, A. (2010). Cenozoic Tectonic Evolution of Asia: A Preliminary Synthesis. *Tectonophysics* 488, 293–325. doi:10.1016/j.tecto.2009.06.002
- Yue, L., Deng, T., Zhang, Y., Wang, J., Zhang, R., and Yang, J. (2004). Magneto Stratigraphy of Stratotype Section of the Baode Stage. *J. Stratigr.* 1, 51–63.
- Zhang, P., Molnar, P., and Downs, W. R. (2001). Increased Sedimentation Rates and Grain Sizes 2–4 Myr Ago Due to the Influence of Climate Change on Erosion Rates. *Nature* 410, 891–897.
- Zhang, S., and Liu, X. (2012). “1:50000 Geological Mapping of Kouquan Fault,” in *Special Inspection Report of Active Fault Earthquake Risk Evaluation Project in Key Surveillance and Defense Area* (Institute of Crustal Stress, China Earthquake Administration Publication). (in Chinese).
- Zhang, Y., and Liao, C. (2006). Transition of the Late Mesozoic–Cenozoic Tectonic Regimes and Modification of the Ordos basin. *Geology. China* 33, 28–40. (in Chinese with English abstract).
- Zhang, Y., Ma, Y., Yang, N., Shi, W., and Dong, S. (2003). Cenozoic Extensional Stress Evolution in North China. *J. Geodynamics* 36, 591–613.
- Zhang, Y. Q., Mercier, J. L., and Vergély, P. (1998). Extension in the Graben Systems Around the Ordos (China), and its Contribution to the Extrusion Tectonics of south China with Respect to Gobi-Mongolia. *Tectonophysics* 285, 41–75. doi:10.1016/s0040-1951(97)00170-4
- Zhao, J., Liu, C., Mountney, N., Lu, J., Cao, J., Yang, Y., et al. (2016). Timing of Uplift and Evolution of the Lüliang Mountains, North China Craton. *Sci. China Earth Sci.* 59 (1), 58–69. doi:10.1007/s11430-015-5153-z
- Zhao, J., Liu, C., Wang, X., Ma, Y., and Huang, L. (2009). Uplift and Evolution Characteristics in the LuLiang Mountain and its Adjacent Area during the Meso-Cenozoic. *Geol. Rev.* 55 (5), 663–672. (in Chinese with English abstract).
- Zheng, D., Zhang, P.-Z., Wan, J., Yuan, D., Li, C., Yin, G., et al. (2006). Rapid Exhumation at ~8 Ma on the Liupan Shan Thrust Fault from Apatite Fission-Track Thermochronology: Implications for Growth of the Northeastern Tibetan Plateau Margin. *Earth Planet. Sci. Lett.* 248, 198–208. doi:10.1016/j.epsl.2006.05.023
- Zhisheng, A., Kutzbach, J. E., Prell, W. L., and Porter, S. C. (2001). Evolution of Asian Monsoons and Phased Uplift of the Himalaya-Tibetan Plateau since Late Miocene Times. *Nature* 411 (6833), 62–66. doi:10.1038/35075035

Conflict of Interest: The authors declare that the research was conducted in the absence of any commercial or financial relationships that could be construed as a potential conflict of interest.

Publisher’s Note: All claims expressed in this article are solely those of the authors and do not necessarily represent those of their affiliated organizations, or those of the publisher, the editors, and the reviewers. Any product that may be evaluated in this article, or claim that may be made by its manufacturer, is not guaranteed nor endorsed by the publisher.

Copyright © 2022 Zhuang, Wei and He. This is an open-access article distributed under the terms of the Creative Commons Attribution License (CC BY). The use, distribution or reproduction in other forums is permitted, provided the original author(s) and the copyright owner(s) are credited and that the original publication in this journal is cited, in accordance with accepted academic practice. No use, distribution or reproduction is permitted which does not comply with these terms.